Carbon 143 (2019) 559–563

Contents lists available at ScienceDirect

Carbon

journal homepage: www.elsevier.com/locate/carbon

Letter to the editor

Electrochemical method for large size and few-layered water-dispersible graphene

A B S T R A C T

We propose an electrochemical route that can prepare few-layered water-dispersible graphene (W-Gr) ≤ 6 atomic layers in thickness and 1–50 μm in lateral size with a remarkably high yield (99%). Simultaneously, high dispersibility (2.5 mg mL^{-1}) and excellent stability (over 6 months) of the W-Gr solution were achieved. All these are attributed to the rational design of electrolyte (NaOH + PTA) and choosing of HOPG as the anode, which ensures enhanced anode oxidation and exfoliation of the large size graphite precursor. This large size W-Gr was used to obtain surface enhanced Raman scattering (SERS) for Rhodamine 6G (R6G) (10^{-8} M).

Graphene dispersions are expected to provide electrically conducting inks particularly suited for flexible electronics and highly thermally conducting coatings [1]. As a 2D macromolecule, its physical and chemical properties critically depend on its lateral size and structural uniformity. The preparation of large size graphene with effective and green dispersion has been a great challenge. Currently, pristine graphene can hardly disperse in water and can only be dispersed in high boiling point organic solvents such as NMP and DMF. However, these organic solvents have the disadvantages of high toxicity and high price. Grafting specific hydrophilic functional groups such as carboxylic, hydroxyl and epoxy groups [2] on graphene is an essential approach to realize W-Gr. Electrochemical exfoliation which does not requires any strong acid and oxidant has emerged as a promising method to produce high-quality graphene for it is low cost, eco-friendly and highly efficient [3]. Essentially, traditional electrochemical exfoliation involves three stages: intercalation of anions/cations, expansion of graphite layers and exfoliation. However, the obtained graphene is generally hydrophobic, thick, and with low oxygen content (<10 at. %) [4]. So, sonication is required as an auxiliary treatment to further strip graphene which will inevitably lead to the decrease of size (5 μm [5]). Our previous work [8] demonstrated a novel strategy for enhancing anodic oxidation through a p-phthalic acid (PTA) coverage on the electrode (graphite foil) to prepare W-Gr. However, the action of the sonication results in a small sheet area of 1.0–7.0 μm^2 (about 1–2.5 μm in lateral size). Hence, preparing W-Gr with high yield, large lateral size and good water dispersibility is of great significance.

Herein, based on our previous work, we replace graphite foil with HOPG to realize enhancing anodic oxidation and inhibiting rapid exfoliation. PTA is rationally selected as electrolyte and plays a very important role in the electrochemical exfoliation of HOPG. PTA is a kind of weak acid that needs NaOH to favor its dissolution in water. When a DC voltage of +10 V is applied on the anode, PTA molecules surrounding the anode precipitate out from NaOH due to the locally reduced pH around the anode ($4OH^- \rightarrow 2H_2O + 4e^- + O_2$), which partially cover the anode surface. The loss of effective anode area as a consequence of PTA coverage means a smaller current density indicating the suppression of anode reactions (mainly the electrolysis of water to generate oxygen bubbles). More importantly, suppressed anode reactions mean slower bubble generation and slower stripping process, which would allow prolonged oxidation of the exposed anode surface to obtain enough water dispersibility. Then the free radicals ($HO^\bullet$ and $O^\bullet$) generated at anode would selectively etch the anode edges without PTA coverage. Next, gas eruption (O_2) exerts large shearing forces on the corroded edges, leading to sheet exfoliation and gradual anode thinning.

Under the same electrolytic condition, the stripping rate of HOPG is much lower than that of graphite foil, and it is calculated to be 0.01429 g/h and 0.04181 g/h, respectively (Fig. S1). This can be ascribed to that HOPG has a higher density (2.86 g/cm^3) than graphite foil (1.12 g/cm^3) (Fig. S2). Without sonication, the present work acquires huge breakthrough in the preparation of large size and few-layered W-Gr. The layer can be controlled in 1–3 layers (78.94%), and size range of 1–50 μm which is up to 10 times of traditional electrochemical methods. The oxygen content of the W-Gr is as high as 24.08 at. % with a C/O ratio of 3.15. The yield is up to 99%, and the concentration is 2.5 mg mL^{-1} over 6 months without obvious aggregation. For fabrication of SERS substrate, the W-Gr was deposited on the surface of the SiO_2/Si substrate and then soaked in R6G aqueous solutions. After soaking, the samples were washed with ethyl alcohol and then dried for the SERS experiment.

Fig. 1a shows a SEM image of W-Gr sheets. It is observed that the W-Gr sheets have a wide size distribution (1–50 μm) (Fig. 1b, Fig. S5). In this work, we have acquired ultra -high yield and large

https://doi.org/10.1016/j.carbon.2018.11.058
0008-6223/

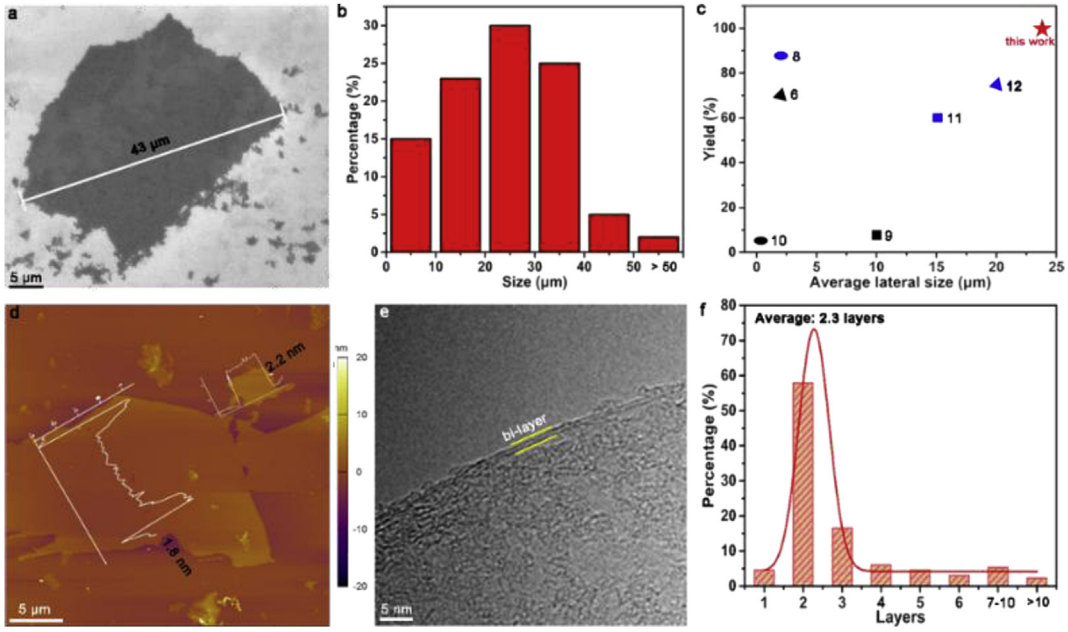

Fig. 1. (a) SEM image and (b) size distribution histograms of W-Gr sheets (c) comparison of yields and lateral size of graphene using HOPG (black spots) [6,9,10] and graphite foil (blue spots) [8,11,12] as anodes (d) AFM image and height profiles (e) HRTEM image and (f) layers with the Gaussian fitting curve of W-Gr sheets. (A colour version of this figure can be viewed online.)

average lateral size, as summarized in Fig. 1c. The typical AFM image (Fig. 1d, Fig. S7) shows the irregular shape of the obtained W-Gr sheets with the lateral size over 30 μm. The thickness is 1.8 nm and 2.2 nm (Fig. 1d) calculated from the topographic height difference between the graphene and the substrate, suggesting approximately 2–3 atomic layers in thickness [6]. High-resolution transmission electron microscopic (HRTEM) images further disclose that the W-Gr sheets range from a single layer to six layers (Fig. 1e and f), mainly 2 layers (Fig. S6). Remarkably, more than 78.94% of W-Gr sheets comprise few-layered graphene (≤3 layers) with an average of 2.3 layers (Fig. 1f). Compared to our previous work [8], this work replaces graphite foil with HOPG and is no need of sonication. As can be seen in Fig. S3, the stripping product of HOPG is large size graphene which indicates that graphene sheets are peeled off layer by layer. However, products of graphite foil contain both thick graphite flakes and small size graphene due to its loose structure and rapid detachment from anode (Fig. S4). And the following 1h sonication required to reduce the thickness results in smaller lateral size (average size: 2 μm) and still lower yield (87.3%) [8]. Due to much denser structure of HOPG that allow complete electrochemical exfoliation (require no post-sonication) and adequate oxidation, we acquire much higher yield (99%) and larger size (1–50 μm) of W-Gr. Considering the lower stripping rate of HOPG which indicates the more efficient electrochemical process, the large lateral size and ultra-high yield can be attributed to the HOPG which has denser structure and much larger composing graphene sheets than graphite foil.

Raman spectrum of both W-Gr and HOPG is shown in Fig. 2a. Compared with HOPG, W-Gr has obvious D peak for a large number of functional groups are grifted to it. The XRD patterns of HOPG and W-Gr powder are shown in Fig. 2b. The sharp peak at $2\theta = 27.0^{\circ}$ of the raw HOPG corresponds to the (002) planes with an interlayer space of 0.33 nm. Whereas for W-Gr, the intensive peak disappears and is replaced with a broadened graphite diffraction hump ranging in 15–37°. This indicates the lack of the long-range order between graphene sheets. The intense crystalline peak of W-Gr occurs at $2\theta = 10.8^{\circ}$. This is the characteristic peak of GO with a d spacing of 0.818 nm. It indicates that graphene sheets have been grifted with abundant oxygen functional groups which can play an essential part in increasing the layer-spacing.

FTIR spectra (Fig. 2c) shows O-H stretching vibration (3221 cm^{-1}), C=C skeletal vibration (1620 cm^{-1}), C-OH stretching vibration (1374 cm^{-1}) and C-O vibration (1043 cm^{-1}) which from another side proved the oxidation process during the anodization. The relatively weak peak at 1740 cm^{-1} may correspond to stretching vibrations of C=O groups [15]. This result is in accordance with the XPS spectrum of C 1s (Fig. 2f) of W-Gr, in which the content of carboxyl/carbonyl groups is relatively low. TGA and DSC provide further evidence for high oxygen degree of W-Gr (Fig. 2d). As can be seen in TG, the total weight loss between RT and 700 °C is 40%. Between RT and 140 °C mainly H_2O (13 wt.%) is released, followed by CO_2 and CO (13 wt.%) which come from decomposition of oxygen-containing functional groups in the temperature range of 140–220 °C where CO_2 dominates. A further weight loss of 11 wt.% that originates from CO and CO_2 occurs between 220 and 475 °C where CO dominates. At higher temperatures (475–700 °C) the weight loss is caused by CO formation (3 wt.%) [14]. The DSC data reveals exothermic events occurring between RT and 700 °C. It reaches a peak at 175 °C as indicated by the intense exothermic process. And this intense exothermic process is accompanied by a sharp weight loss which corresponds to the TG sharp decline between 140 and 220 °C. There is also an obvious decline in TG between 220 and 475 °C but with no obvious DSC peak. This is because that the exothermic process is relatively smooth and steady. As is shown in Fig. 2e, an obvious O 1s peak was detected in the XPS spectrum of W-Gr. The peaks at 285.0 eV and 533.0 eV are attributed to the C 1s and O 1s peak, respectively. The oxygen content is as high as 24.08 at. % with a C/O ratio of 3.15. In this paper, graphene aerogel with three-dimensional architecture by freezing drying the W-Gr dispersions and the corresponding SEM characterization were conducted (Fig. S9). This is a convincing evidence for

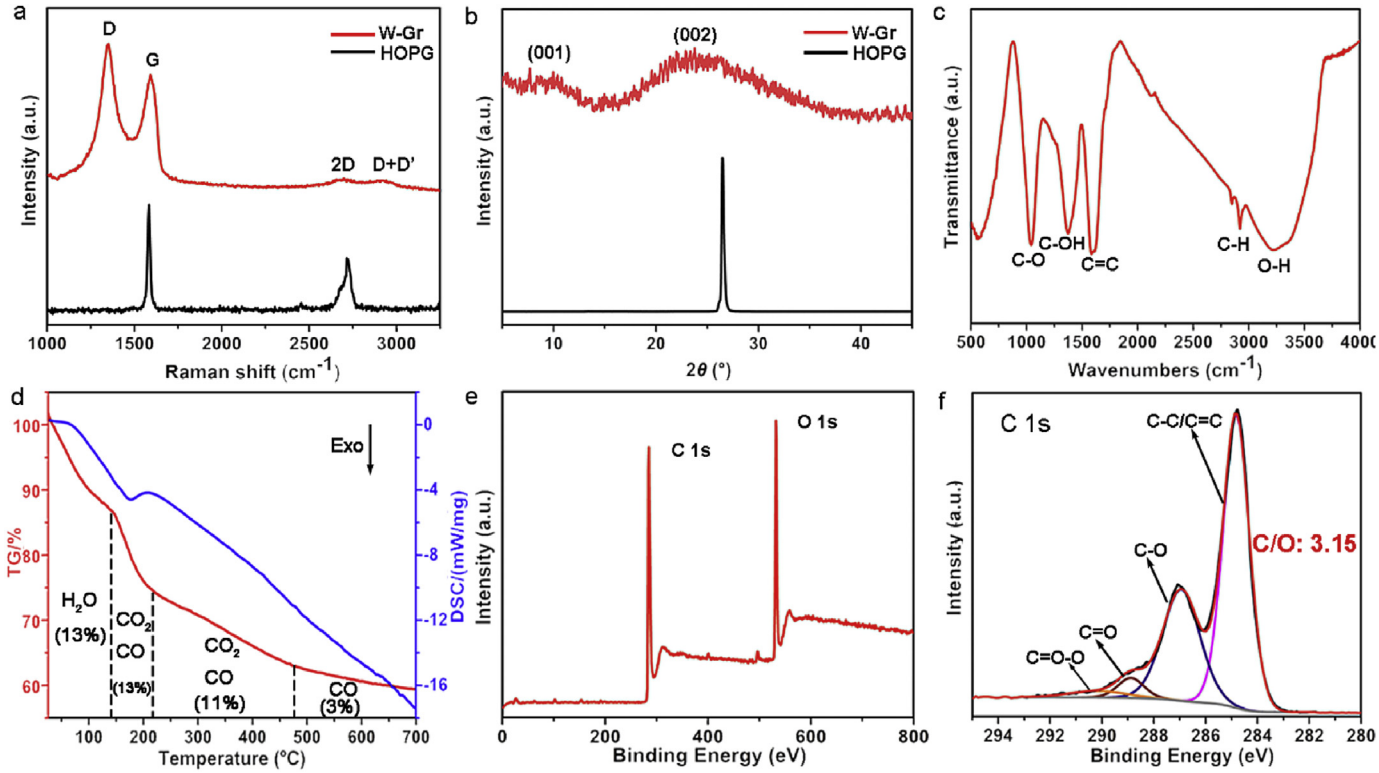

Fig. 2. (a) Raman and (b) XRD of both HOPG and W-Gr (c) FT-IR spectrum (d) TGA and DSC spectra (e) XPS survey spectra and (f) XPS C 1s spectrum of W-Gr. (A colour version of this figure can be viewed online.)

strong interaction force between W-Gr sheets which comes from high oxygen degree of W-Gr. According to the high-resolution spectrum of C 1s (Fig. 2f), four different peaks located at 290.4 eV, 288.8 eV, 286.8 eV and 284.7 eV were attributed to C=O-O, C=O, C-O (hydroxyl and epoxy) groups and C=C/C-C bonds, respectively. As expected, the XPS result confirms the successful grafting of oxygen functional groups on the obtained W-Gr sheets during the electrochemical process.

The UV–Vis spectrum of W-Gr presents a strong peak at 264 nm (π-π^* transition of the conjugation domains) and a weak peak at 310 nm (n-π^* transition of the carbonyl groups) (Fig. 3a). Distinct Tyndall effect is observed in W-Gr aqueous solution (the inset). This reveals the excellent dispersibility and stability of W-Gr in water. The high Zeta potential of −43.5 mV (Fig. 3b) can also explain the stabilization of W-Gr aqueous solution. The whole characterization above confirms that stable few-layered W-Gr was realized through this electrochemical approach with a lateral size of several tens of micrometers.

The W-Gr of large size (1–50 μm) is exceptionally suitable for the practical use as SERS substrate [7]. For comparison, we prepared R6G-soaked GO and R6G-soaked W-Gr and obtained a Raman spectrum on them (Fig. 4a). For GO, only D peak and G peak are observed, no R6G characteristic peaks at all. On the contrast, there are distinct R6G characteristic peaks in the W-Gr Raman spectrum, and this is vital for identification of molecules. Obviously, the W-Gr studied here is a much better SERS substrate.

Fig. 4b shows a series of Raman spectra of R6G on the surface of

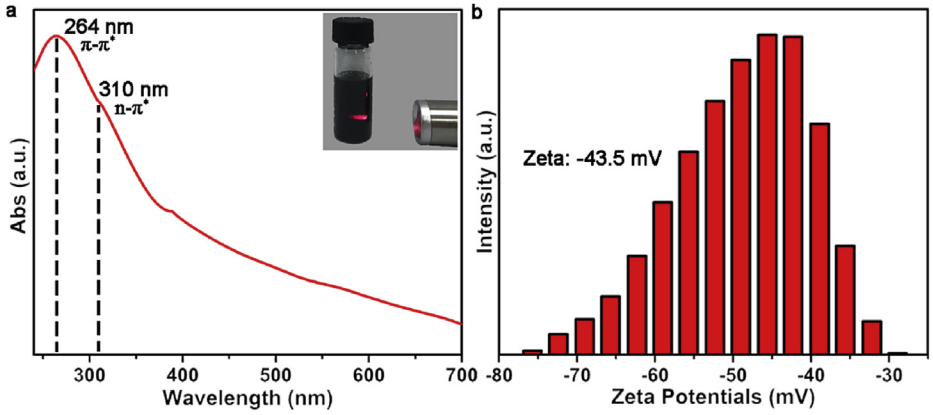

Fig. 3. (a) UV–Vis spectrum of W-Gr aqueous solution and the inset shows the Tyndall Effect (b) Zeta potential of W-Gr dispersion. (A colour version of this figure can be viewed online.)

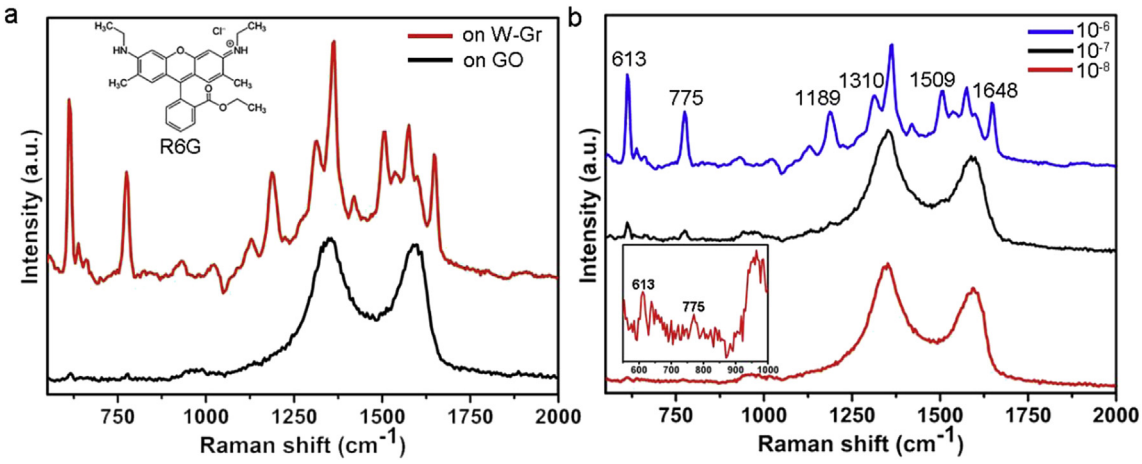

Fig. 4. (a) Raman spectrum of R6G on W-Gr (red line) compared with that on GO (black line). 10^{-6} M R6G aqueous solution was used to load the fluorescent molecule on both W-Gr and GO. (b) Raman spectra of R6G on the W-Gr. A series of soaking concentrations: 10^{-6} M (blue line), 10^{-7} M (black line), and 10^{-8} M (red line). The inset corresponds to 10^{-8} M R6G on W-Gr. (A colour version of this figure can be viewed online.)

W-Gr, which can be identified definitely by the main peaks of the vibration modes at 613, 775, 1189, 1310, 1509 and 1648 cm^{-1}. The signals were found to monotonically diminish with the decreased concentration. It shows that the Raman signals can still be clearly detected even at a very low concentration of R6G (10^{-8} M). This low detection level is comparable to that of CVD N-doped graphene [13]. It should be stressed that R6G is a dye molecule with an intensive fluorescence background and is difficult to detect through conventional Raman at such low concentrations. However, the vibration fingerprints of R6G can be clearly observed on W-Gr despite the low soaking concentration. As is shown in Fig. S8, the Raman signals of R6G on W-Gr are found to decrease with the increasing number of W-Gr layers. The simple and low-cost electrochemical stripping process makes W-Gr easy to realize industrial production.

As for the mechanism of SERS, the results mentioned above indicate that the difference in the Raman enhancement should be attributed to the intrinsic nature of the substrate and its interaction with the probe molecule. According to the high-resolution spectrum of C 1s (Fig. 2f), three oxygen-containing groups C=O-O, C=O and C-O groups are favorable for the Raman enhancement. It is understandable because the related oxygen-containing groups possess a strong local dipole moment that can induce a considerable local electric field under the laser excitation [7]. Such an enhanced electric field could naturally result in the enhancement of the Raman signals.

In conclusion, the problem of thick layer caused by fast traditional electrochemical stripping is solved through enhanced slow anodic oxidation and inhibited rapid incomplete exfoliation. Without sonication, the layer can be controlled in 1–3 layers (78.94%), and size range of 1–50 μm which is up to 10 times of traditional electrochemical method. The oxygen content is as high as 24.08 at. % with a C/O ratio of 3.15. The yield is 99%, and the concentration is 2.5 mg mL^{-1}. This large size W-Gr can be used to obtain surface enhanced Raman scattering for R6G (10^{-8} M).

Acknowledgements

The authors thank Dr. Li Wei of TESCAN China for providing RISE Instrument support and his great suggestions and help in SEM and Raman measurements. This work was supported by the National Natural Science Foundation of China (Grants 51802337, 11774368, 11704204 and 11804353), China Postdoctoral Science Foundation (Grant BX201700271) and STCSM (18511110600).

Appendix A. Supplementary data

Supplementary data to this article can be found online at https://doi.org/10.1016/j.carbon.2018.11.058.

References

[1] D. Ager, V.A. Vasantha, R. Crombez, J. Texter, Aqueous graphene dispersions–optical properties and stimuli-responsive phase transfer, ACS Nano 8 (11) (2014) 11191–11205.
[2] S. Tian, S. Yang, T. Huang, J. Sun, H.S. Wang, X.P. Pu, et al., One-step fast electrochemical fabrication of water-dispersible graphene, Carbon 111 (2017) 617–621.
[3] P. He, H. Gu, G. Wang, S.W. Yang, G.Q. Ding, Z. Liu, et al., Kinetically enhanced bubble-exfoliation of graphite towards high-yield preparation of high-quality graphene, Chem. Mater. 29 (20) (2017) 8578–8582.
[4] S. Yang, S. Brüller, Z.S. Wu, Z. Liu, K. Parvez, R. Dong, et al., Organic radical-assisted electrochemical exfoliation for the scalable production of high-quality graphene, J. Am. Chem. Soc. 137 (43) (2015) 13927–13932.
[5] S. Yang, A.G. Ricciardulli, S. Liu, R. Dong, M.R. Lohe, A. Becker, et al., Ultrafast delamination of graphite into high-quality graphene using alternating currents, Angew. Chem. Int. Ed. 56 (23) (2017) 6669–6675.
[6] J. Wang, K.K. Manga, Q. Bao, K.P. Loh, High-yield synthesis of few-layer graphene flakes through electrochemical expansion of graphite in propylene carbonate electrolyte, J. Am. Chem. Soc. 133 (23) (2011) 8888–8891.
[7] X. Yu, H. Cai, W. Zhang, X. Li, N. Pan, Y. Luo, et al., Tuning chemical enhancement of SERS by controlling the chemical reduction of graphene oxide nanosheets, ACS Nano 5 (2) (2011) 952–958.
[8] H. Wang, S.Y. Tian, S.W. Yang, X.F. You, L.X. Xu, Q.T. Li, et al., Anode coverage for enhanced electrochemical oxidation: a green and efficient strategy towards water-dispersible graphene, Green Chem. 20 (6) (2018) 1306–1315.
[9] C.Y. Su, A.Y. Lu, Y.P. Xu, F.R. Chen, A.N. Khlobystov, L.J. Li, High-quality thin graphene films from fast electrochemical exfoliation, ACS Nano 5 (3) (2011) 2332–2339.
[10] J. Lu, J.X. Yang, J.Z. Wang, A. Lim, S. Wang, K.P. Loh, One-pot synthesis of fluorescent carbon nanoribbons, nanoparticles, and graphene by the exfoliation of graphite in ionic liquids, ACS Nano 3 (8) (2009) 2367–2375.
[11] A.M. Abdelkader, I.A. Kinloch, R.A.W. Dryfe, Continuous electrochemical exfoliation of micrometer-sized graphene using synergistic ion intercalations and organic solvents, ACS Appl. Mater. Interfaces 6 (3) (2014) 1632–1639.
[12] L. Wu, W. Li, P. Li, S. Liao, S. Qiu, M. Chen, et al., Powder, paper and foam of few-layer graphene prepared in high yield by electrochemical intercalation exfoliation of expanded graphite, Small 10 (7) (2014) 1421–1429.
[13] S. Feng, C.D.S. Maria, R.C. Bruno, R. Lv, F. Kazunori, L.E. Ana, et al., Ultrasensitive molecular sensor using N-doped graphene through enhanced Raman scattering, Sci Adv 2 (7) (2016).
[14] S. Eigler, C. Dotzer, A. Hirsch, M. Enzelberger, P. Müller, Formation and

decomposition of CO_2 intercalated graphene oxide, Chem. Mater. 24 (7) (2012) 1276–1282.
[15] E.S. Orth, J.E.S. Fonsaca, S.H. Domingues, H. Mehl, M.M. Oliveira, A.J.G. Zarbin, Targeted thiolation of graphene oxide and its utilization as precursor for graphene/silver nanoparticles composites, Carbon 61 (61) (2013) 543–550.

Huixia Tang
State Key Laboratory of Functional Materials for Informatics, Shanghai Institute of Microsystem and Information Technology, Chinese Academy of Sciences, Shanghai, 200050, PR China

School of Physical Science and Technology, ShanghaiTech University, Shanghai, 200031, PR China

CAS Center for Excellence in Superconducting Electronics (CENSE), Shanghai, 200050, PR China

University of Chinese Academy of Sciences, Beijing, 100049, PR China

Peng He*, Tao Huang
State Key Laboratory of Functional Materials for Informatics, Shanghai Institute of Microsystem and Information Technology, Chinese Academy of Sciences, Shanghai, 200050, PR China

CAS Center for Excellence in Superconducting Electronics (CENSE), Shanghai, 200050, PR China

University of Chinese Academy of Sciences, Beijing, 100049, PR China

Ziyang Cao
School of Materials Science and Engineering, University of Shanghai for Science and Technology, Shanghai, 200093, PR China

Penglei Zhang
State Key Laboratory of Functional Materials for Informatics, Shanghai Institute of Microsystem and Information Technology, Chinese Academy of Sciences, Shanghai, 200050, PR China

CAS Center for Excellence in Superconducting Electronics (CENSE), Shanghai, 200050, PR China

University of Chinese Academy of Sciences, Beijing, 100049, PR China

Gang Wang
Department of Microelectronic Science and Engineering, Faculty of Science, Ningbo University, Ningbo, 315211, PR China

Xianying Wang
School of Materials Science and Engineering, University of Shanghai for Science and Technology, Shanghai, 200093, PR China

Guqiao Ding**
State Key Laboratory of Functional Materials for Informatics, Shanghai Institute of Microsystem and Information Technology, Chinese Academy of Sciences, Shanghai, 200050, PR China

CAS Center for Excellence in Superconducting Electronics (CENSE), Shanghai, 200050, PR China

University of Chinese Academy of Sciences, Beijing, 100049, PR China

Xiaoming Xie
State Key Laboratory of Functional Materials for Informatics, Shanghai Institute of Microsystem and Information Technology, Chinese Academy of Sciences, Shanghai, 200050, PR China

School of Physical Science and Technology, ShanghaiTech University, Shanghai, 200031, PR China

CAS Center for Excellence in Superconducting Electronics (CENSE), Shanghai, 200050, PR China

University of Chinese Academy of Sciences, Beijing, 100049, PR China

* Corresponding author. State Key Laboratory of Functional Materials for Informatics, Shanghai Institute of Microsystem and Information Technology, Chinese Academy of Sciences, Shanghai, 200050, PR China.

** Corresponding author. State Key Laboratory of Functional Materials for Informatics, Shanghai Institute of Microsystem and Information Technology, Chinese Academy of Sciences, Shanghai, 200050, PR China.
E-mail address: hepeng@mail.sim.ac.cn (P. He).
E-mail address: gqding@mail.sim.ac.cn (G. Ding).

28 September 2018
Available online 26 November 2018